Dalton Transactions

ROYAL SOCIETY OF CHEMISTRY

PAPER

View Article Online
View Journal | View Issue

Cite this: *Dalton Trans.*, 2021, **50**, 5506

Scrutinising the role of intramolecular hydrogen bonding in water exchange dynamics of Gd(III) complexes†

Loredana Leone, [a] Sara Camorali,[a] Antía Freire-García,[b] Carlos Platas-Iglesias, *[b] David Esteban Gomez [b] and Lorenzo Tei *[a]

We report a series of structurally related Gd(III) complexes designed to modulate the exchange of the coordinated water molecule, which is an important parameter to be controlled to achieve optimal performance of contrast agents for application in magnetic resonance imaging (MRI). The ligands contain a DO3A scafold functionalised with 2′-methoxyphenacyl or 4′-methoxyphenacyl groups (DO3A-*o*MAP and DO3A-*p*MAP), a 2′-aminophenacyl group (DO3A-*o*AnAP) or a 2′,4′-dihydroxyphenacyl moiety (DO3A-DiHAP). The results are compared with those obtained previously for the analogues containing 2′- or 4′-hydroxyphenacyl groups (DO3A-*o*HAP and DO3A-*p*HAP, respectively) and the parent system with an unsubstituted acetophenone pendant arm (DO3A-AP). ^{1}H NMR studies performed on the Eu(III) complexes show that ligand functionalisation causes a very minor effect on the relative populations of the SAP and TSAP isomers present in solution, with the SAP isomer representing 70–80% of the overall population. The emission spectra of the Eu(III) complexes confirm the presence of a water molecule coordinated to the metal center and point to similar coordination environments around the metal ion. The analysis of the ^{1}H NMRD profiles and ^{17}O NMR data recorded for the Gd(III) complexes evidences that water exchange is modulated by the ability of peripherical substituents to establish hydrogen bonds with the coordinated and/or second sphere water molecules. DFT calculations were used to model the transition states responsible for the dissociative water exchange mechanism, providing support to the crucial role of hydrogen-bonds in accelerating water exchange.

Received 20th January 2021,
Accepted 29th March 2021

DOI: 10.1039/d1dt00204j

rsc.li/dalton

Introduction

Magnetic resonance imaging (MRI) is a powerful diagnostic technique widely used to obtain detailed anatomical functional images of the human body. As a further tool to highlight certain pathologies, MRI contrast agents (CAs) are often required in order to increase the contrast between the healthy tissue and the lesion. Nowadays, clinically employed CAs are low molecular weight Gd(III) complexes with linear or macrocyclic polyaminocarboxylate ligands, which are capable to enhance the longitudinal relaxation rate of water protons in the human tissues.[1,2] The increase of the longitudinal relaxation rate, induced by one millimolar concentration of the paramagnetic ion, is called relaxivity (r_1) and it depends on several structural and dynamic features of the Gd(III) complex.[3] Some of these key parameters are the rotational correlation time (τ_R), which relates to the molecular size and stereochemical rigidity of the complex, and the residence lifetime of the coordinated water molecule(s) (τ_M) in exchange with the bulk water.[1,2] The latter parameter, can be also expressed as $k_{ex} = 1/\tau_M$ where k_{ex} is the exchange rate of the water molecule coordinated to the metal centre. Water exchange can be modulated by modifying the structural and electronic features of the complex and it can be determined by variable-temperature ^{17}O-NMR studies.[4]

A useful strategy for the design of an efficient MRI CA relies on the structural modification on the pendant arms of one of the most investigated macrocyclic ligands, DOTA (DOTA = 1,4,7,10-tetraazacyclododecane-1,4,7,10-tetraacetate). The Gd(III) complex of DOTA is used as a contrast agent in clinical practice under the name DOTAREM®.[3] For example, the pres-

[a]*Dipartimento di Scienze e Innovazione Tecnologica (DiSIT). Università degli Studi del Piemonte Orientale "Amedeo Avogadro", Viale T. Michel 11, I-15121 Alessandria, Italy. E-mail: lorenzo.tei@uniupo.it*

[b]*Centro de Investigacións Científicas Avanzadas (CICA) and Departamento de Química, Facultade de Ciencias, Universidade da Coruña, 15071 A Coruña, Galicia, Spain. E-mail: carlos.platas.iglesias@udc.es*

† Electronic supplementary information (ESI) available: ^{1}H NMR spectra, absorption and emission spectra, additional r_1 and ^{17}O NMR data and geometries obtained with DFT calculations. See DOI: 10.1039/d1dt00204j

ence of functional groups forming hydrogen-bonds with the coordinated water molecule,[5] or with second sphere water molecules in proton exchange with a coordinated hydroxyl group,[6] have been recently shown to lead to an increase in the relaxivity of small molecular weight Gd(III) complexes. However, in these examples the H-bond formation did not involve modulation of k_{ex}.

In a recent work,[7] we have explored two novel chelators consisting of DO3A (1,4,7,10-tetraazacyclododecane-1,4,7-triacetic acid), bearing 2′-hydroxyphenacyl and 4′-hydroxyphenacyl groups respectively as the fourth pendant arm (DO3A-*o*HAP and DO3A-*p*HAP, Scheme 1). Our results showed that GdDO3A-*o*HAP is endowed with a higher k_{ex} due to its capability to form hydrogen bonds between the *ortho*-phenol(ate) groups and the water molecules involved in the dissociative exchange mechanism, thus stabilizing the eight-coordinate transition state. On the other hand, GdDO3A-*p*HAP, with the phenol(ate) group pointing outwards from the complex, had k_{ex} values similar to the model system GdDO3A-AP, which lacks H-bond acceptor groups. In the present work, we expand this family of macrocyclic ligands by changing the nature of the H-bond donor group and/or increasing their number on the aromatic moiety of the ligand. Therefore, we have synthesised and characterised four new DO3A-AP-like ligands with a fourth pendant arm consisting of 2′-methoxyphenacyl or 4′-methoxyphenacyl groups (DO3A-*o*MAP and DO3A-*p*MAP), a 2′-aminophenacyl group (DO3A-*o*AnAP) or a 2′,4′-dihydroxyphenacyl moiety (DO3A-DiHAP, Scheme 1). The main aim of this study is to evaluate the impact on k_{ex} and relaxivity of changing the nature of the H-bond donor group ($-NH_2$ *vs.* –OH), and whether further substitution of the aromatic ring can also influence these properties (DO3A-DiHAP). The derivatives containing –OMe groups were designed as controls, as they lack H-bond donor groups. Spectroscopic studies using ^{1}H NMR and absorption and emission electronic spectroscopy were carried out to gain information on the structures of the complexes in solution. A DFT study was also conducted to rationalise the trends observed in exchange rates of the coordinated water molecule.

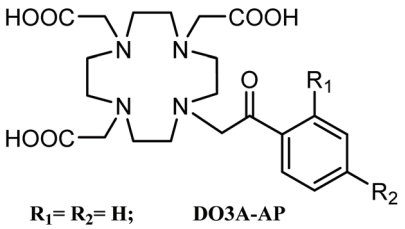

R_1= R_2= H; DO3A-AP
R_1= OH, R_2= H; DO3A-*o*HAP
R_1= H, R_2= OH; DO3A-*p*HAP
R_1= OMe, R_2= H; DO3A-*o*MAP
R_1= H, R_2= OMe; DO3A-*p*MAP
R_1= NH_2, R_2= H; DO3A-*o*AnAP
R_1= OH , R_2= OH; DO3A-DiHAP

Scheme 1 DO3A-acetophenone (DO3A-AP) and their derivatives discussed in the present work.

Results and discussion

Synthesis

Ligands DO3A-*o*MAP, DO3A-*p*MAP, DO3A-*o*AnAP and DO3A-DiHAP were synthesised following the procedure reported in Scheme 2. In particular, the synthesis started from the reaction of DO3A(^{t}Bu)$_3$ with *o*- or *p*-methoxy-2-bromoacetophenone to obtain the *ortho* and *para*-methoxy derivatives DO3A(^{t}Bu)$_3$-*o*, *p*MAP. Trifluoroacetic acid deprotection of the *tert*-butyl esters yielded the DO3A-*o*MAP and DO3A-*p*MAP ligands. On the other hand, to obtain the DO3A-*o*AnAP derivative, DO3A(^{t}Bu)$_3$ was reacted first with *o*-nitro-2-bromoacetophenone, followed by reduction of the nitro group with H_2 on Pd/C to obtain the amino derivative. Subsequent trifluoroacetic acid deprotection gives the third ligand DO3A-*o*AnAP. Regarding the last chelator, DO3A-DiHAP, reaction of DO3A(^{t}Bu)$_3$ with commercially available 2′,4′-dihydroxy-2-bromoacetophenone yielded DO3A(^{t}Bu)$_3$-DiHAP, and the final ligand was obtained by deprotection of the *t*-butyl esters by TFA/DCM (1 : 1). This reaction mixture was then concentrated in vacuum and purified by preparative HPLC-MS. Complexation of the free ligands was accomplished by using the lanthanide trichloride salts (Ln(III) = Gd, Eu) in water at pH 7. Free lanthanide ion excess was eliminated by precipitation and filtration of the hydroxide at basic pH.

Spectroscopic study on Eu(III) complexes

To get more insight into the structural and dynamic properties of Ln-DO3A-*o*AnAP, LnDO3A-DiHAP and LnDO3A-MAP complexes, the Eu(III) complexes were investigated by using ^{1}H NMR spectroscopy at three temperatures (283, 298 and 310K, ESI†). In case of EuDO3A-DiHAP, the ^{1}H NMR spectra at pH 4 and 9 showed that the (de)protonation of the phenol does not change substantially the ratio of the isomers present in solution (Fig. S1†). Thus, in this work all other spectroscopic measurements were recorded only at neutral pH. The solution structure of these DO3A-acetophenone-like complexes is expected to resemble that of the corresponding LnDOTA complexes.[8] The latter complexes are characterised by the presence of two different coordination isomers defined by the same conformation of the macrocyclic ring but with different orientation of the side arms (*i.e.*, capped square-antiprismatic geometry, SAP, and capped twisted square antiprismatic geometry, TSAP). These isomers exhibit two different sets of signals in the paramagnetic ^{1}H NMR spectra with a relative population that is affected by the size of the Ln(III) ion.[8] The substitution of one acetic arm with substituted phenacyl moieties reduces the symmetry removing the proton equivalence, although the carbonyl oxygen is expected to coordinate the metal ion and therefore the rigidity of the system should be maintained. The ^{1}H NMR spectra of EuDO3A-DiHAP and EuDO3A-*o*AnAP at pH 7 and at 283 K (Fig. S2 and S3†) show one predominant set of signals (70–80%) and another set present in *ca.* 20–30% amount. The chemical shifts of the four predominant axial ring protons are in the range 25–40 ppm, suggesting the presence of SAP isomers.[9] By comparing the integral of the two sets of signals of axial ring-protons, the ratio between the SAP

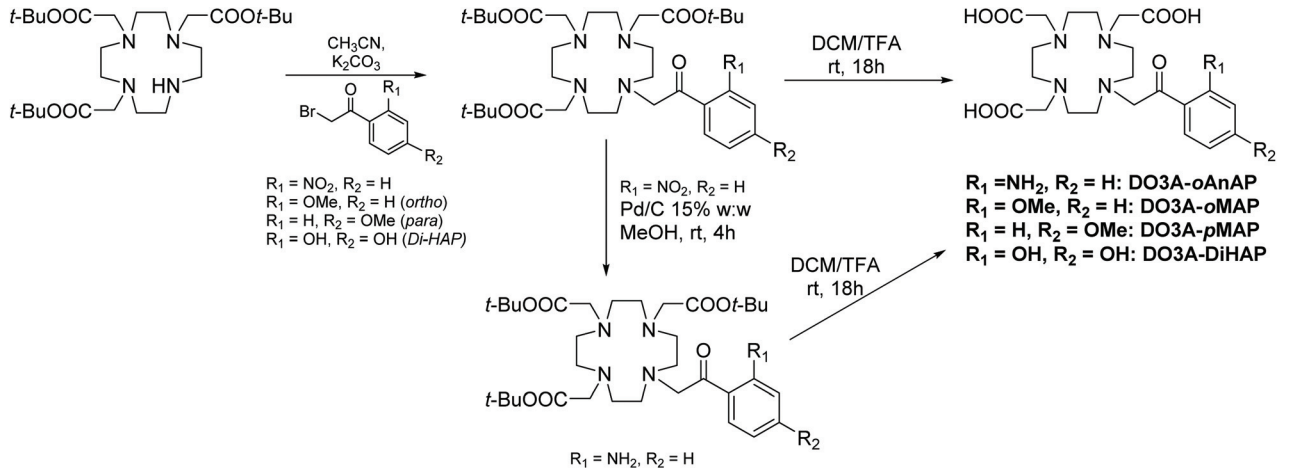

Scheme 2 Synthetic route followed for the preparation of the ligands.

and TSAP isomers for EuDO3A-*o*AnAP and EuDO3A-DiHAP at neutral pH can be estimated as about 76 : 24 and 75 : 25, respectively. For the other Eu-complexes (Fig. S4 and S5†) the SAP/TSAP ratio were 76 : 24 for EuDO3A-*o*MAP and 82/18 for EuDO3A-*p*MAP.

The emission spectra of the Eu(III) complexes with DO3A-*o*HAP, DO3A-*p*HAP and DO3A-*o*AnAP are characterised by very weak emission intensities associated to the $^5D_0 \rightarrow {}^7F_J$ transitions (J = 0–4) typical of the complexes with this metal ion (Fig. S10–S14, ESI†).[10] The lifetimes of the excited $^5D_0$ state measured in water (τ_{H_2O}) fall within the range 0.39–0.51 ms (Table 1). The emission quantum yields determined for these complexes with hydroxyl or amine substituents on the acetophenone group are very low (<1.6%, Table 1).

The complexes with the ligands containing methoxyl substituents show however rather strong luminescence, with emission quantum yields of ~6–7%. The quantum yield determined for EuDO3A-*p*MAP (6.9%) compares reasonably well with the value reported in the literature (9.8%),[11] considering the uncertainty of these measurements. The EuDO3A-*o*,*p*MAP complexes are also characterised by longer lifetimes of the Eu(III) $^5D_0$ excited state (0.63 ms, Table 1). The latter values are in the upper range of the lifetimes reported for monohydrated DO3A Eu(III) derivatives (*ca.* 0.33–0.68 ms).[12–14] The lifetimes of the $^5D_0$ excited state were also measured in D_2O solution to estimate the number of coordinated water molecules using the expressions developed by Horrocks and Beeby.[15,16] This analysis afforded hydration numbers close to 1 for all complexes with substituents at position 4 of the phenyl ring. The EuDO3A-*o*AnAP and EuDO3A-*o*HAP complexes present somewhat higher calculated hydration numbers, likely due to the deactivation effect caused by the –OH and $-NH_2$ groups involved in hydrogen bonds with the oxygen atom of the acetophenone moiety.

The low quantum yields determined for the complexes with DO3A-*o*,*p*HAP and DO3A-*o*AnAP are likely related to a poor efficiency of the energy transfer, associated to a low energy of the ligand-centred triplet state. Indeed, the absorption spectra of these complexes show maxima at rather low energy (λ_{max} >335 nm, Table 1). Application of the methodology developed by Werts to this family of structurally related complexes leads to similar radiative lifetimes of Eu(III), τ_{rad}, which fall in the range 9.3–10.1 ms.[17] The comparable values of τ_{rad} obtained suggests similar coordination environments around the metal ion. The analysis of the photophysical data indicates that the low quantum yields of the DO3A-*o*,*p*HAP and DO3A-*o*AnAP complexes is related to low sensitisation efficiencies, η_{sens}, which are however virtually quantitative in the case of the EuDO3A-*o*,*p*MAP complexes, in agreement with previous data.[11]

The emission spectra of all complexes are characterised by a rather intense $^5D_0 \rightarrow {}^7F_0$ transition, which can be attributed to the low symmetry of the crystal field originated by the

Table 1 Absorption and emission properties of the Eu(III) complexes[a]

Ligand	λ_{max}/nm	τ_{H_2O}/ms	τ_{D_2O}/ms	Φ_{Eu}/%	q^c	$\Delta J = 2$: $\Delta J = 1$	τ_{rad}/ms	η_{sens}/%
DO3A-*o*MAP	338/267	0.630(1)	2.285(1)	6.0	1.1	0.95	10.1	0.96
DO3A-*p*MAP	306	0.628(1)	2.243(1)	6.9/9.8[b]	1.1	1.10	9.5/6.65[b]	1.0/0.99[b]
DO3A-*o*AnAP	396/271	0.389(2)	0.91(1)	<0.2	1.5	1.12	9.4	~0.04
DO3A-*o*HAP	337/266	0.510(2)	2.104(7)	0.4	1.5	0.96	9.8	0.08
DO3A-*p*HAP	352/306	0.456(3)	0.814(5)	1.6	0.9	1.13	9.3	0.33
DO3A-AP[b]	265	0.62	2.26	0.6	1.1	—	7.37	0.71

[a] Conditions provided in Fig. 1. [b] Data from ref. 11. [c] Calculated according to ref. 16.

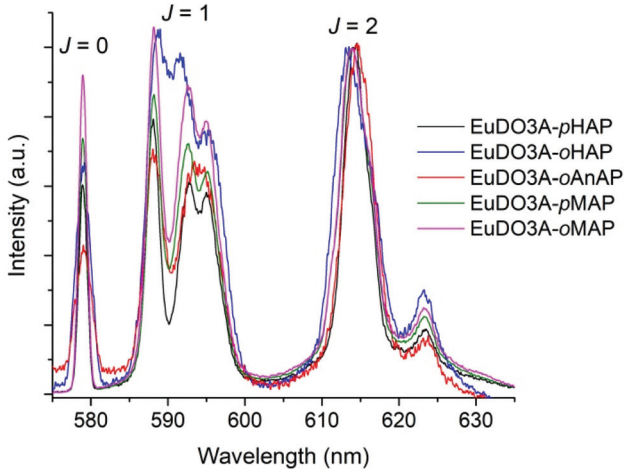

Fig. 1 Partial emission spectra of the Eu(III) complexes normalised to the intensity of the $^5D_0 \rightarrow {}^7F_2$ transition. Conditions: EuDO3A-*p*HAP (10^{-4} M, pH 5.1, λ_{exc} = 314 nm, bandpass = 1 nm); EuDO3A-*o*HAP (pH 4.9, λ_{exc} = 350 nm, bandpass = 2 nm); EuDO3A-*o*AnAP (pH 7.4, λ_{exc} = 400 nm, bandpass = 2 nm); EuDO3A-*p*MAP (pH 7.4, λ_{exc} = 312 nm, bandpass = 1 nm); EuDO3A-*o*MAP (pH 7.4, λ_{exc} = 350 nm, bandpass = 1 nm).

coordination of the ligand. The presence of three components for the $^5D_0 \rightarrow {}^7F_1$ transition is also in line with a low symmetry.[18] The emission profile is also characterised by similar ratios of the $\Delta J = 2$ and $\Delta J = 1$ transitions (0.95–1.13, Table 1). The intensity of the magnetic dipole $^5D_0 \rightarrow {}^7F_1$ transition is virtually independent of the metal coordination environment, while the electric dipole character of the $^5D_0 \rightarrow {}^7F_2$ transition makes it very sensitive to variations in the metal coordination sphere.[12,19] Thus, the similar $\Delta J = 2/\Delta J = 1$ intensity ratios point to similar structures of the complexes in solution. For instance, significant changes in the $\Delta J = 2/\Delta J = 1$ intensity ratios (from 0.6 to 5.2) were observed upon changing the axial donor in Eu(III) DOTA-tetraamide complexes.[19] The complexes also show very similar splitting of the $^5D_0 \rightarrow {}^7F_1$ transition, with the exception of the EuDO3A-*o*HAP complex. The energies of the three components observed for the EuDO3A-*o*AnAP, EuDO3A-*o*,*p*MAP and EuDO3A-*p*HAP complexes with respect to the $^5D_0 \rightarrow {}^7F_0$ transition are 270 ± 6, 403 ± 2 and 468 ± 2 cm^{-1}. The corresponding values measured for EuDO3A-*o*HAP are 296, 371 and 473 cm^{-1} (Table S1, ESI†). Since all these complexes present similar populations of the SAP and TSAP isomers in solution, the different splitting of the $^5D_0 \rightarrow {}^7F_1$ manifold in EuDO3A-*o*HAP must be related to subtle structural changes of the metal coordination environment.

pH dependence

The pH dependence of the relaxivity (r_1) of Gd(III) complexes of this class of DO3A-like ligands was measured to assess the possible change in r_1 with (de)protonation of the functional group(s) on the aromatic ring (Fig. 2A). For GdDO3A-*o*,*p*MAP the r_1 *vs.* pH graphs show no evident change in r_1 in the range of pH 2–12 and thus a retention of the coordination sphere of the metal ion in this pH range. As for GdDO3A-*o*AnAP and GdDO3A-DiHAP, the relaxivity varies slightly in the range of pH 2–12. It drops from pH 2 to pH 7 and then slightly rises towards basic pH for GdDO3A-*o*AnAP. In the case of GdDO3A-DiHAP, the relaxivity rises slightly from pH 5 to pH 11. These results show that: (i) for GdDO3A-*o*AnAP, the protonation of the aromatic amine can cause an increase in relaxivity due to a small contribution of second-sphere water molecules hydrogen bonded to the protonated amine or to an acid-catalysed proton exchange contribution;[6] (ii) the deprotonation

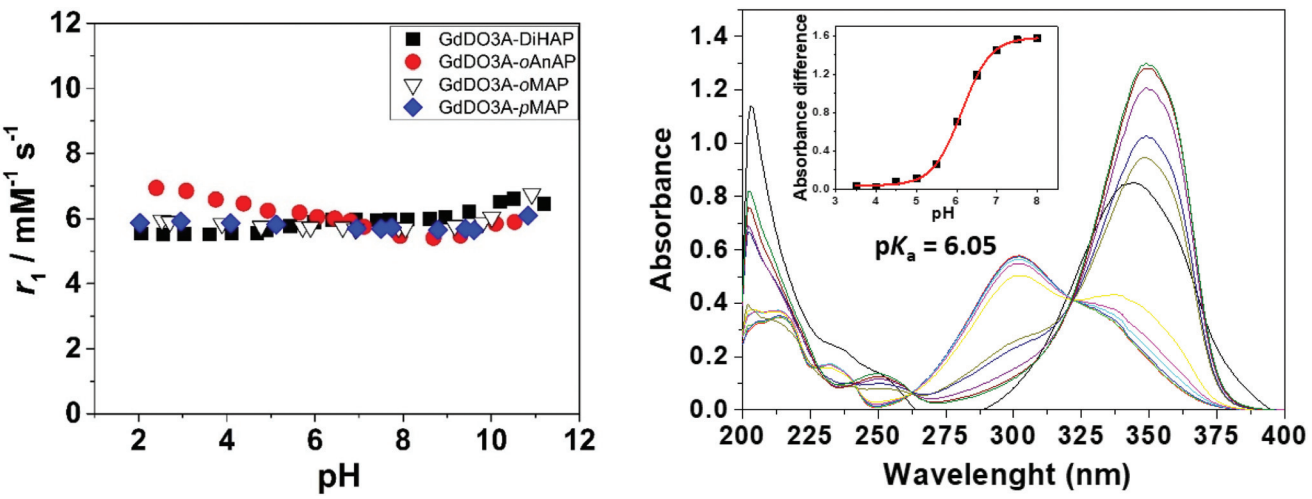

Fig. 2 Left: Plots of ^1H relaxivity for GdDO3A-AP-derivatives as a function of pH (20 MHz and 298 K); right: UV spectra (λ = 200–450 nm) of GdDO3A-DiHAP (4×10^{-4} M) in different aqueous buffer solutions ranging from pH 4.5 to 9.9. The absorbances are normalized to zero for λ = 600 nm. Insert: Plot of the total absorbance difference *vs.* pH to determine the pK_a. The total absorbance difference is the sum of the absolute absorbance difference values at the chosen wavelengths (*i.e.* 300 and 350 nm). The pK_a value was worked out by nonlinear regression as reported in ref. 20.

of the dihydroxyphenyl moiety leads to a small r_1 increase, probably due to the formation of a negatively charged, more hydrophilic complex.

In order to get further insight on the pH dependence, we carried out variable pH UV-vis measurements on the free ligands and on the correspondent Gd(III)-complexes. In case of the DO3A-DiHAP ligand, the –OH deprotonation results in a red shift of the absorption band from 280 to 340 nm, associated to a pK_a of 6.93 ± 0.09 (0.1 M NaCl, 298 K, Fig. S15†), whereas the GdDO3A-DiHAP complex shows a shift from 300 to 350 nm and a pK_a of 6.05 ± 0.04 (Fig. 2B). The ΔpK_a of ≈0.88 units can be attributed to an electron withdrawing effect of the metal ion that allows the delocalization of the negative charge also on the carbonyl oxygen, in part forming an enolate anion. In the case of DO3A-*o*AnAP, the absorption spectra did not experience changes with pH, and thus it was not possible to determine the pK_a in the chosen working range.

Relaxometric properties

To the best of our knowledge, except for our previous communication,[7] relaxometric studies on Gd-complexes having a ketone donor group have not been reported so far. We could only find the relaxivity values at 20 MHz, 310 K and pH 7.0 for a di- and a tri-nuclear Gd-complex with phenyl-di- (or tri-) acyl groups connecting two or three DO3A moieties. The r_1 values were 6.1 mM^{-1} s^{-1} for the trinuclear system and 5.4 mM^{-1} s^{-1} for the dinuclear analogue.[21] On the other hand, the other reported LnDOTA-like chelates bearing a pendant arm with a ketone donor have been used for luminescence studies.[11,22–24] Sherry and co-workers reported another interesting study on Eu(III)-ketone coordination, demonstrating slow water exchange induced by the coordination of the carbonyl oxygen due to its lower electron density with respect to amide or carboxylate oxygen donors.[25]

As discussed above, in case of the dihydroxyphenacyl derivatives the coordination of the Gd(III) ion changes in the physiological pH range with deprotonation of the –OH group and delocalization of the negative charge to form an enolate anion that coordinates the metal ion. However, the variation of r_1 from basic to acidic pH observed was very small. This means that either there is no change in the structural and dynamic parameters related to the Gd-complex, or that counteracting variations in different parameters do not alter r_1 significantly. In our previous study, the detailed ^{17}O NMR analysis at acidic and basic pH of GdDO3A-*o*HAP showed that water exchange dynamics are not substantially affected by pH changes, therefore, in the present work we focused on determining the relaxometric properties of the complexes at physiological pH. Thus, the r_1 values for GdDO3A-*o*AnAP, GdDO3A-DiHAP and GdDO3A-*o*,*p*MAP at 20 MHz, 298 and 310 K and pH 7.4 are listed in Table 2. The r_1 values are consistent with the presence of one coordinated water molecule (q = 1), although the r_1 values are slightly higher than the values measured in analogous conditions for other q = 1 Gd-complexes of comparable molecular weight. As r_1 depends on the magnetic field strength, temperature, and several important molecular parameters of the paramagnetic metal complex, a complete ^{1}H and ^{17}O NMR relaxometric study was carried out to obtain detailed information of the physicochemical properties of the complexes. Thus, the variation of r_1 as a function of the magnetic field strength, the so-called nuclear magnetic resonance dispersion profile (^{1}H NMRD), was measured for all complexes at 298, and 310 K in the proton Larmor frequency range 0.01–120 MHz, corresponding to magnetic field strengths varying between 2.34×10^{-4} and 3 T (Fig. 3 and S16, ESI†). The profiles show the characteristic shape of a low molecular weight Gd-complex with a plateau at low fields, a dispersion around 4–8 MHz, and another plateau with lower relaxivity in the high-frequency region (>20 MHz). This behaviour is quite typical for Gd chelates whose relaxivity is largely dominated by rotational dynamics.[26]

The temperature dependence of the solvent ^{17}O NMR transverse relaxation rates, R_2, and shifts, $\Delta\omega$, allowed obtaining more accurate and quantitative information on the kinetics of

Table 2 Best-fit parameters obtained from the analysis of the $1/T_1$ ^{1}H NMRD profiles (298 and 310 K) and ^{17}O NMR data for GdDO3A-AP, GdDO3A-*o*AnAP, GdDO3A-*o*HAP (at pH 4), GdDO3A-*p*HAP, GdDO3A-*o*MAP and GdDO3A-*p*MAP[a]

Complex	Isomer	$^{298}r_1$[b] (mM^{-1} s^{-1})	$^{310}r_1$[b] (mM^{-1} s^{-1})	$^{298}\tau_R$ (ps)	$^{298}\tau_M$ (ns)	Δ^2 (10^{19} s^{-2})	$^{298}\tau_v$ (ps)	E_M (kJ mol^{-1})
GdDO3A-*o*MAP	SAP	5.7 ± 0.1	5.0 ± 0.1	93 ± 2	1050 ± 10	4.5 ± 0.1	5.1 ± 0.1	51 ± 1
	TSAP				6.5 ± 1.0	4.3 ± 0.3	3.2 ± 0.3	71 ± 4
GdDO3A-*p*MAP	SAP	5.7 ± 0.1	5.1 ± 0.2	90 ± 3	1100 ± 20	5.4 ± 0.3	5.8 ± 0.2	52 ± 1
	TSAP				11.0 ± 1.2	4.7 ± 0.2	3.8 ± 0.4	80 ± 3
GdDO3A-*o*AnAP	SAP	5.3 ± 0.1	4.6 ± 0.2	91.6 ± 2.3	690 ± 10	5.0 ± 0.4	5.2 ± 0.3	51 ± 2
	TSAP				15.5 ± 1.1	4.6 ± 0.3	6.8 ± 0.4	57 ± 5
GdDO3A-DiHAP	SAP	5.4 ± 0.2	4.7 ± 0.2	81.8 ± 0.7	695 ± 5	4.6 ± 0.2	5.1 ± 0.2	52 ± 1
	TSAP				8.5 ± 0.7	10 ± 0.5	5.0 ± 0.1	57 ± 3
GdDO3A-AP[c]	SAP	5.1	4.6	100	1200	9.8	5.1	58.9
	TSAP				25	5.0	14.8	50
GdDO3A-*o*HAP[c]	SAP	6.4	5.4	105	210	8.5	5.7	34
	TSAP				2.2	3.0	24.8	40
GdDO3A-*p*HAP[c]	SAP	5.8	4.9	95	950	7.0	5.8	54
	TSAP				7.1	3.3	3.4	32

[a] The parameters fixed in the fitting procedure are: q = 1, r_{GdO} = 2.5 Å, r_{GdH} = 3.0 Å, a_{GdH} = 4.0 Å, $^{298}D_{GdH}$ = 2.25×10^{-5} cm^2 s^{-1}, E_R = 16 kJ mol^{-1}, E_v = 1 kJ mol^{-1}, $A/\hbar$ = -3.0×10^6 rad s^{-1}. [b] Relaxivities at 20 MHz. [c] From ref. 7.

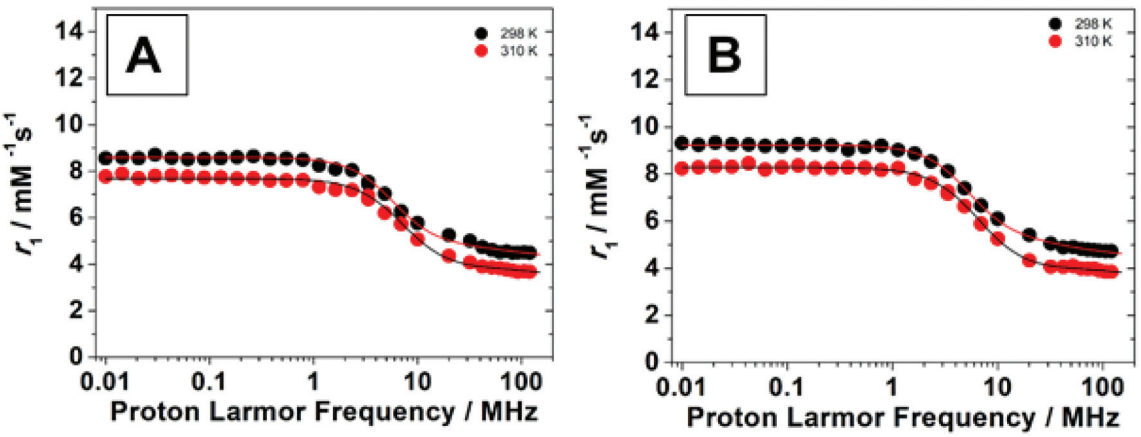

Fig. 3 ^{1}H NMRD profiles recorded at 298 (black) and 310 K (red) for (A) GdDO3A-*o*AnAP at pH 7.4 and (B) GdDO3A-DiHAP at pH 7.4.

water exchange (measurements at 11.75 T on 10–20 mM solutions of the complexes at physiological pH). For all chelates the resulting profiles of ^{17}O R_2 *vs.* T (Fig. 4 and S17, ESI†) suggest the presence of two species with very different water exchange dynamics. In fact, the shapes of the curves are distant from the simple pseudo-exponential trend expected for systems containing one coordinated water molecule in exchange with the bulk solvent. As already shown for GdDO3A-*o*,*p*HAP and GdDO3A-AP,[7] the two species present in solution can be considered the SAP and TSAP isomers observed in the ^{1}H NMR spectra of the corresponding Eu-complexes. Similar observations were recently reported for GdHPDO3A and derivatives[27,28] and previously for two GdDOTA-bisamide complexes.[29] These studies demonstrated that the TSAP isomer, present in lower concentration, has a water exchange lifetime significantly shorter than that observed for the SAP isomer. Notably, in all chelates discussed in the present work, the contributions of the TSAP isomers become important for T < 290 K and predominant at lower temperatures. In particular, in the profiles of the reported Gd-complexes, the R_2 values are almost steady from 275 to 290 K, increase with temperature from 290 to 320–330 K, where a maximum is observed, and then they decrease at higher temperatures. These profiles contain contributions from a small amount of fast exchanging TSAP isomer that is hidden behind the larger portion of slow exchanging SAP isomer, which gives the peak at 320–330 K rather typical of Gd-chelates characterized by a long water exchange lifetime (τ_M ~1 μs), *i.e.* GdDOTA-monoamides.[30] The ^{17}O R_2 profiles recorded for GdDO3A-*o*MAP and GdDO3A-*p*MAP present a maximum at about the same temperature, anticipating very similar k_{ex} values (Fig. S17†). This maximum is slightly shifted to lower temperatures for GdDO3A-*o*AnAP and GdDO3A-DiHAP, which indicates that water exchange is slightly faster for the dominant SAP isomer. A more pronounced effect was observed previously for the GdDO3A-*o*HAP complex, where the phenol(ate) group assisted the k_{ex} increase by H-bonding with water molecules involved in the exchange process.[7]

The variable-temperature ^{17}O R_2 profiles were fitted according to the well-established set of Swift–Connick equations[31] using a model that considers the presence in solution of two

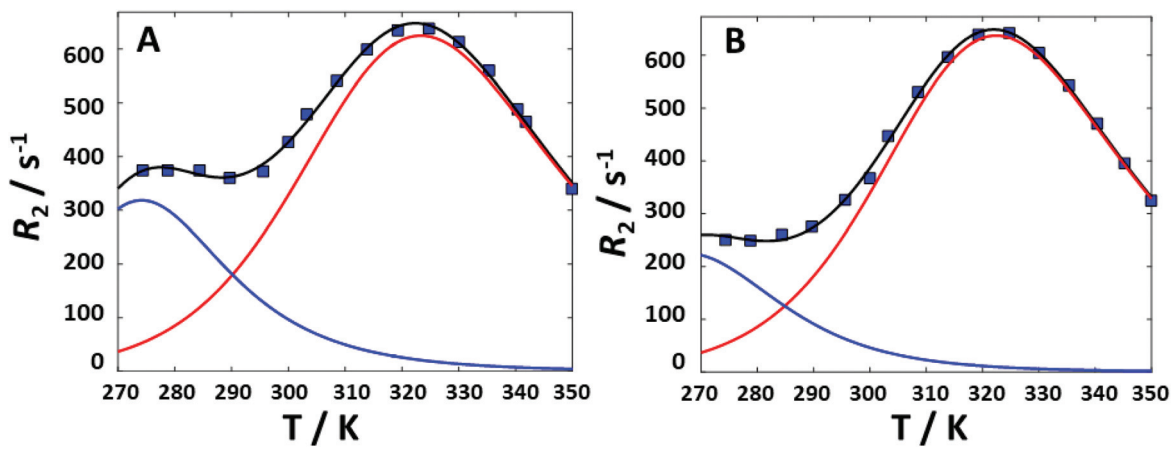

Fig. 4 Transverse ^{17}O relaxation rates measured at 11.74 T and pH 7.4 for: (A) GdDO3A-*o*AnAP (9.6 mM) and (B) GdDO3A-DiHAP (15.9 mM). The red and blue lines represent the calculated contributions of the isomeric species SAP and TSAP, respectively.

isomeric species whose relative population is extrapolated from the ^{1}H NMR spectra of the Eu-complexes (the TSAP/SAP ratio is considered constant over the range of temperatures under examination, Fig. S1–S5, ESI†). Moreover, the NMRD data were analysed using the standard Solomon Bloembergen Morgan model for the inner-sphere relaxation mechanism[32] and Freed's model for the outer-sphere components.[33] The water exchange parameters that affect the inner-sphere contribution were fixed at weighted averages of the values obtained for the two isomers by fitting the ^{17}O NMR data (Table 2). Given the large number of parameters involved in the fitting, some of them were fixed to known or reasonable values as shown in Table 2. The rotational correlation time τ_R, considering that two isomers have similar rotational dynamics, was determined for all complexes by fitting the NMRD profiles. Values in the range 80–105 ps were found, in agreement with τ_R values reported for Gd-complexes of analogous molecular volume.[34] The parameters associated with the electronic relaxation times $T_{1,2e}$ (Δ^2 and τ_V) are also in line with the values obtained previously for similar complexes.[27,30] Noteworthy, in the case of GdDO3A-DiHAP at pH 7.4, a mixture of species are present, neutral and anionic, so the parameters obtained represent an average between those of the two species.

The τ_M values obtained for the SAP isomers (0.69–1.1 μs) are longer than those determined for the TSAP isomers (τ_M in the 6.5–15.5 ns range), in line with previous results.[35] This has been attributed to the steric compression around the water binding site in the TSAP isomers, which facilitates the departure of the water molecule following a dissociatively activated water exchange mechanism.[4] The τ_M values determined for the (dominant) SAP isomers of the structurally-related Gd(III) complexes listed in Table 1 fall in three categories: the GdDO3A-*o*MAP, GdDO3A-*p*MAP and GdDO3A-*p*HAP complexes display $^{298}\tau_M$ values of ~0.9–1.1 μs, which indicates that the incorporation of –OMe substituents, or a –OH group in *para* position, do not have a significant effect in the exchange rate of the water molecule ($^{298}\tau_M$ = 1.2 μs for the unsubstituted GdDO3A-AP derivative). A second group encompasses the GdDO3A-DiHAP and GdDO3A-*o*AnAP complexes, with $^{298}\tau_M$ values of ~0.7 μs. Finally, water exchange is considerably faster for GdDO3A-*o*HAP ($^{298}\tau_M$ ~0.2 μs).

DFT calculations

DFT calculations were conducted to rationalise the different water exchange rates observed for the Gd(III) complexes listed in Table 2. Our calculations focused on the more abundant SAP isomers, for which water exchange rates were determined to a higher accuracy. Following our previous studies, a few explicit second-sphere water molecules were introduced in the models, together with a polarized continuum to account the effects of bulk water. The inclusion of explicit second-sphere water molecules was found to be critical to obtain accurate Gd–O_{water} distances and ^{17}O hyperfine coupling constants $A/\hbar$.[36,37]

Geometry optimizations performed for the GdDO3A-*o*MAP and GdDO3A-*p*MAP complexes provided metal coordination environments very similar to the parent (unsubstituted) GdDO3A-AP complex (see Computational details below, and Table S2, ESI†). Noteworthy, the methoxy substituent in GdDO3A-*o*MAP points outside the coordination sphere of the complex, as a result of steric hindrance (Fig. S36, ESI†). Thus, it is not surprising that the three complexes present similar exchange rates of the coordinated water molecule.

Geometry optimizations performed for the Gd(III) complexes of DO3A-*o*HAP, DO3A-*o*AnAP and DO3A-DiHAP yield very similar distances between the metal ion and the oxygen atom of the coordinated water molecule (r_{GdO}, Table 3). Furthermore, the complex with DO3A-AP shows a similar calculated r_{GdO} value compared with the functionalised derivatives, in spite of the lower water exchange rate of the former. The r_{GdO} values were found previously to correlate reasonably well with the water exchange rate in nine-coordinate Gd(III) complexes, with a longer distance, and thus a weaker coordination, generally corresponding to a faster exchange.[38] Thus, we conclude that additional factors not related to the strength of the Gd–O_{water} bond are responsible for the different water exchange rates. The ^{17}O hyperfine coupling constants ($A/\hbar$) of the coordinated water molecules obtained from scalar relativistic calculations are also very similar (~3×10^6 rad s^{-1}, Table 3), and equal to the value assumed for the analysis of the ^{17}O NMR shifts and relaxation data ($A/\hbar = -3.0 \times 10^6$ rad s^{-1}, see above).

The main difference among the different calculated structures is related to the Gd–O bond distance involving the carbonyl oxygen atom of the acetophenone group (Table S2, ESI†), which takes values of 2.429 (GdDO3A-*o*AnAP), 2.443 (GdDO3A-DiHAP), 2.456 (GdDO3A-*o*HAP), 2.465 (GdDO3A-*o*MAP) and 2.481 Å (GdDO3A-AP). These Gd–O distances correlate with the activating ability of the substituents of the aromatic ring (NH_2 > OH > OMe > H).[39] These structural changes are however not likely responsible for the different splitting pattern of the $^5D_0 \rightarrow {}^7F_1$ transition observed for GdDO3A-*o*HAP, as all other complexes, including GdDO3A-*o*AnAP, show a similar splitting of the $^7F_1$ level. Interestingly, the complex showing a distinct splitting in the emission spectrum is that showing very fast water exchange. While we do not have a definitive explanation for this effect, the fast dissociative water exchange may

Table 3 Water exchange parameters and ^{17}O hyperfine coupling constants of the coordinated water molecules obtained with DFT calculations for the GdDO3A-AP, GdDO3A-*o*HAP, GdDO3A-*o*AnAP and GdDO3A-DiHAP complexes[a]

	DO3A-AP	DO3A-*o*HAP	DO3A-*o*AnAP	DO3A-DiHAP
r_{GdO}/Å	2.516	2.516	2.523	2.518
r_{GdO} (TS)/Å	3.471	3.337	3.237	3.247
$\Delta H^{\ddagger}$/kJ mol^{-1}	28.9	22.6	25.9	24.5
$\Delta S^{\ddagger}$/J K^{-1} mol^{-1}	+2.7	+16.4	+10.8	+12.7
$\Delta G^{\ddagger}_{298}$/kJ mol^{-1}	28.1	17.7	22.68	20.7
$A_O/\hbar/10^6$ rad s^{-1}	2.6	2.7	3.0	2.7

[a] Data obtained from calculations on the GdDO3A-AP·3H_2O, GdDO3A-*o*HAP·4H_2O, GdDO3A-DiHAP·4H_2O and GdDO3A-*o*AnAP·3H_2O systems.

cause the complex to spend a non-negligible time in the dehydrated state.[40] Since the crystal field splitting of cyclen-based complexes containing four pendant arms is very sensitive to axial ligation,[19,41] a significant population of the dehydrated form is expected to impact the splitting of the $^7F_1$ level.

The potential energy surfaces of the complexes were explored by increasing the r_{GdO} distance in steps of 0.05 Å from the equilibrium geometry to ~4 Å. This eventually led to a second energy minimum for each complex in which the Gd(III) ion is eight-coordinated. Subsequently, we optimized the transition states that relate the nine- and eight-coordinated forms of the complexes, as models for the dissociative water exchange reaction (Fig. 5). The structures of the transition states obtained for the complexes with DO3A-*o*HAP, DO3A-*o*AnAP and DO3A-DiHAP show that the water molecule that is leaving the metal coordination environment is involved in hydrogen-bonds with the –OH/NH_2 groups of the ligand. On the contrary, the leaving water molecule in GdDO3A-AP enlarges the r_{GdO} distance from 2.516 to 3.471 Å on going from the ground to the transition state but remains in the axial position. The energy barriers computed with DFT are characterised by positive activation entropies, as expected for a dissociative water exchange mechanism.[42] The calculated $\Delta H^{\ddagger}$ and $\Delta G^{\ddagger}$ values follow the trend observed for water exchange, with GdDO3A-AP showing the highest energy barrier for water exchange and GdDO3A-*o*HAP the lowest. The GdDO3A-DiHAP and GdDO3A-*o*AnAP complexes present intermediate values for both $\Delta H^{\ddagger}$ and $\Delta G^{\ddagger}$. We notice that while the experimental

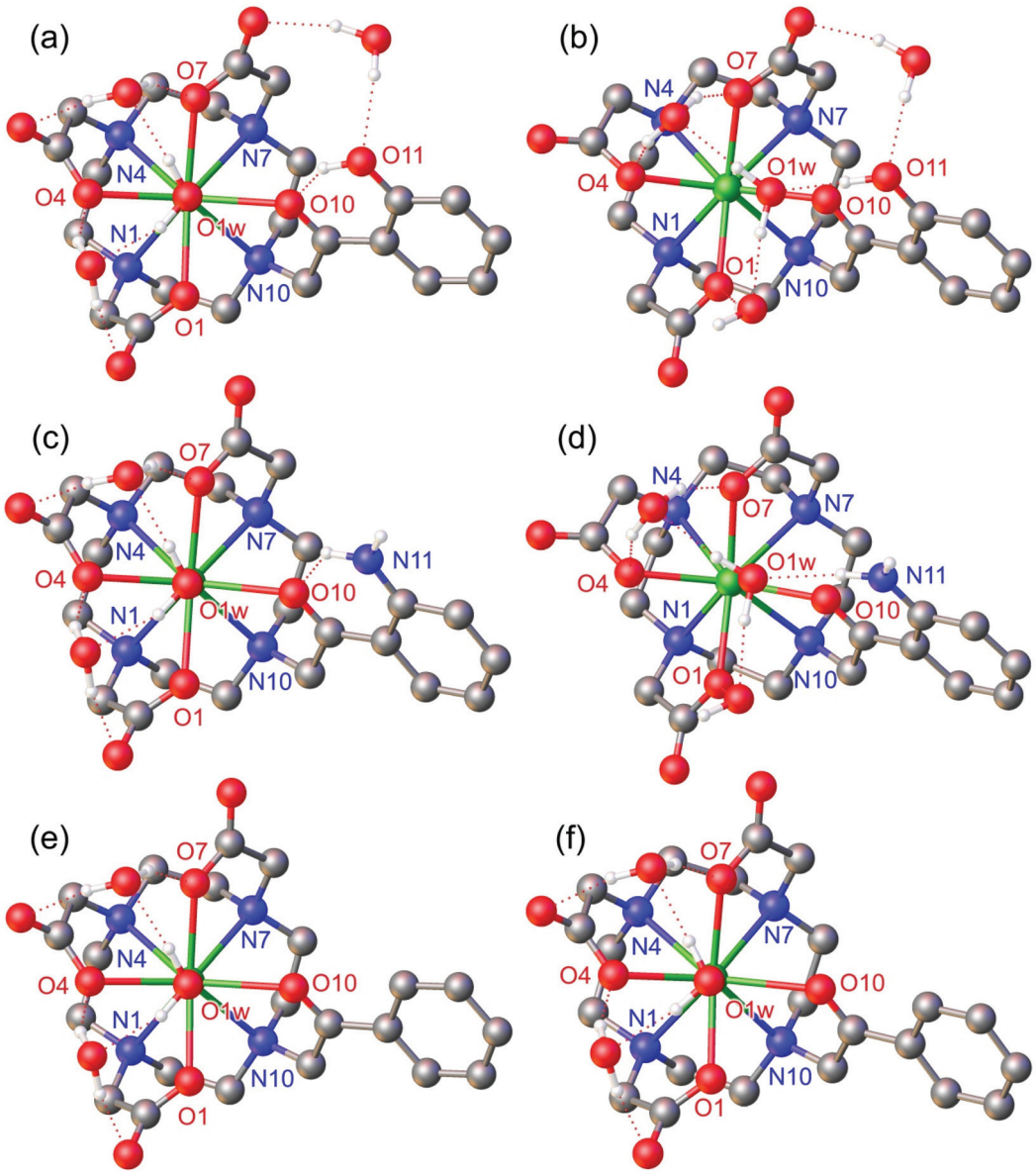

Fig. 5 Structures of the ground states (left panel) and transition states (right panel) optimized with DFT calculations for the GdDO3A-*o*HAP·4H_2O (a and b), GdDO3A-*o*AnAP·3H_2O (c and d) and GdDO3A-AP·3H_2O (e and f) systems.

Table 4 Hydrogen bonding data obtained with DFT calculations for the minimum energy geometries and transition states of the GdDO3A-AP, GdDO3A-*o*HAP, GdDO3A-*o*AnAP and GdDO3A-DiHAP complexes[a]

	DO3A-*o*HAP		DO3A-*o*AnAP		DO3A-DiHAP	
	Minimum	TS	Minimum	TS	Minimum	TS
D–H···A/Å	1.688	1.777	1.896	2.067	1.672	2.099
D···A/Å	2.545	2.688	2.618	2.972	2.539	2.883
D–H···A/°	144.0	152.3	126.0	147.6	145.2	135.9

[a] Data obtained from calculations on the GdDO3A-AP·3H_2O, GdDO3A-*o*HAP·4H_2O, GdDO3A-DiHAP·4H_2O and GdDO3A-*o*AnAP·3H_2O systems.

trend is qualitatively well reproduced by our calculations, the calculated activation energies are lower than those obtained from the analysis of the ^{17}O NMR data. We tested different density functionals and found that activation energies are very sensitive to the choice of the functional, while the use of the large-core (4f in core) or small-core pseudopotentials provided very similar results.

The higher barrier calculated for GdDO3A-*o*AnAP compared with GdDO3A-*o*HAP can be reasonably attributed to the weaker hydrogen bonds established in the aniline derivative (Table 4). The –NH_2 group establishes relatively weak intramolecular hydrogen bond with the carbonyl oxygen atom of the acetophenone group in the ground state geometry, as indicated by the N–H···O angle (126°), which is far from the ideal linear value. The hydrogen bond involving the leaving water molecule and the –NH_2 group in the transition state is also weak when compared to that established in the GdDO3A-*o*HAP complex. Unexpectedly, the hydrogen bond established by the –OH group with the leaving water molecule is weaker in GdDO3A-DiHAP compared with GdDO3A-*o*HAP. This is explained by the electron donating effect of the hydroxyl group at position 4, which reinforces the intramolecular hydrogen bond with the carbonyl group in the ground state.

Conclusions

This work has demonstrated that water exchange in Gd(III) complexes can be conveniently modulated by introducing peripheral hydrogen bond donor groups. The water exchange rates are increased by stabilization of the eight-coordinate transition state thanks to the formation of a hydrogen bond between the peripheral substituent and the leaving water molecule. The results reported in this paper provide an additional strategy for fine tuning the physicochemical parameters of Gd(III)-based MRI contrast agents.

Experimental and computational section

General methods

All chemicals were purchased from Sigma-Aldrich or Alfa Aesar unless otherwise stated and were used without further purification. The ^1H and ^{13}C NMR spectra were recorded using a Bruker Avance III 500 MHz (11.4 T) spectrometer equipped with 5 mm PABBO probes and BVT-3000 temperature control unit. Chemical shifts are reported relative to TMS and were referenced using the residual proton solvent resonances. HPLC analyses and mass spectra were performed on a Waters HPLC-MS system equipped with a Waters 1525 binary pump. Analytical measurements were carried out on a Waters XBridge-Phenyl (5 μm 4.6 × 150 mm) column, while a Waters XBridge-Phenyl Prep OBD (5 μm, 19 × 100 mm) column was used for preparative purposes.

HPLC analytical method (Method 1) = A: TFA 0.1% in H_2O; B: MeOH; flow 1 mL min^{-1}; 0–3 min: 1% B, 3–18 min: from 1 to 100% B, 18–19 min 100% B, 19–20 min 1% B. HPLC preparative method (Method 2) = TFA 0.1% in H_2O; B: MeOH; flow 20 mL min^{-1}; 0–3 min: 30% B, 3–13 min: from 30 to 77% B, 13–14 min from 77 to 100% B, 14–16 min 100% B. Electrospray ionization mass spectra (ESI MS) were recorded using a SQD 3100 Mass Detector (Waters), operating in positive or negative ion mode, with 1% v/v formic acid in MeOH as the carrier solvent. DO3A(tBu)$_3$-*o*MAP and DO3A(tBu)$_3$-*p*MAP were synthesized as reported previously.[7]

Synthesis

1-(2-(2-Nitrophenyl)-2-oxoethyl)-4,7,10-tris-(*t*-butoxycarbonyl methyl)-1,4,7,10-tetraazacyclododecane (DO3A(tBu)$_3$-*o*NO_2AP). A solution in CH_3CN (5 mL) of DO3A(tBu)$_3$ (200 mg, 0.39 mmol) K_2CO_3 (100 mg, 0.72 mmol) and 2-bromo-2′-nitroacetophenone (208 mg, 0.80 mmol) was left stirring under N_2 atmosphere for 5 h at room temperature and then filtered, evaporated *in vacuo* and then purified by silica gel chromatography (95 : 5 to 90 : 10 CH_2Cl_2–MeOH) to afford (DO3A(tBu)$_3$-*o*-NO_2AP) (180 mg, 0.26 mmol, yield 67%). ^1H NMR ($CDCl_3$, 500 MHz): δ (ppm) = 8.07 (d, J = 8 Hz, –*m*-Ph–, 1H), 7.73 (d, J = 8 Hz, –*o*-Ph–, 1H), 7.68–7.66 (m, –*m*′,*p*-Ph–, 2H), 3.67–2.09 (m, macrocycle, (–NC$\underline{H}_2$COOC(CH$_3$)$_3$, –N$\underline{CH}_2$COPh, 24H), 1.37 (s, (–NCH$_2$COOC(C$\underline{H}_3$)$_3$, 27H). ^{13}C NMR ($CDCl_3$, 125 MHz): δ (ppm) = 202.4 (NCH$_2$$\underline{CO}$Ph), 173.1 (–NCH$_2$$\underline{CO}$OC(CH$_3$)$_3$), 146.2 (–$C_2$-Ph), 135.3 (–$C_1$-Ph–), 134.2 (–$C_5$-Ph–), 131.5 (–$C_4$-Ph–), 128.0 (–$C_6$-Ph–), 124.5 (–$C_3$-Ph–), 82.0 (–NCH$_2COO\underline{C}$(CH$_3$)$_3$), 63.3 (–N$\underline{C}H_2$COPh), 55.6 (–N$\underline{C}H_2$COOC(CH$_3$)$_3$), 54.7–48.6 (macrocycle), 27.80 (–NCH$_2$COOC(C$\underline{H}_3$)$_3$). ESI-MS (m/z): found 678.5 $[M + H]^+$ (calc for $C_{34}H_{56}N_5O_9$: 678.40).

1-(2-(2-Aminophenyl)-2-oxoethyl)-4,7,10-tris-(*t*-butoxycarbonyl methyl)-1,4,7,10-tetraazacyclododecane (DO3A(tBu)$_3$-*o*AnAP).

After two vacuum/H_2 cycles to replace air inside the reaction vessel with hydrogen, a mixture of (DO3A(tBu)$_3$-*o*-NO_2AP) (180 mg, 0.26 mmol) and Pd/C (15 wt% of the substrate, 27 mg), in MeOH (10 mL) was vigorously stirred at room temperature under 1 atm of H_2 for 4 h. The reaction mixture was filtered through a celite pad and the filtrate was concentrated in vacuum to obtain (DO3A(tBu)$_3$-*o*-NH_2AP) (151 mg, 0.23 mmol, yield 90%). ^{1}H NMR ($CDCl_3$, 500 MHz): δ (ppm) = 7.58 (d, J = 8 Hz, –*m*-Ph–, 1H), 7.23 (t, J = 7.5 Hz, –*p*-Ph–, 1H), 6.74 (d, J = 8.3 Hz, –*o*-Ph–, 1H), 6.57 (t, J = 7.5 Hz, –*m*′-Ph–, 1H), 3.46–2.24 (m, macrocycle, (–NC$\underline{H}_2$COOC(CH$_3$)$_3$, –N$\underline{CH}_2$COPh, 24H), 1.44 (s, (–NCH$_2$COOC(C$\underline{H}_3$)$_3$, 27H). ^{13}C NMR ($CDCl_3$, 125 MHz): δ (ppm) = 200.7 (NCH$_2$$\underline{CO}$Ph), 172.7 (–NCH$_2$$\underline{CO}$OC(CH$_3$)$_3$), 150.56 (–$C_2$-Ph), 134.5 (–$C_4$-Ph–), 129.1(–$C_6$-Ph–), 117.6 (–$C_5$-Ph–), 116.5 (–$C_3$-Ph–), 115.8 (–$C_1$-Ph–), 82.0 (–NCH$_2COO\underline{C}$(CH$_3$)$_3$), 60.1 (–N$\underline{C}H_2$COPh), 56.0 (–N$\underline{C}H_2$COOC(CH$_3$)$_3$), 55.5–48.7 (macrocycle), 27.80 (–NCH$_2$COOC(C$\underline{H}_3$)$_3$). ESI-MS (m/z): found 648.4 [M + H]$^+$ (calc for $C_{34}H_5N_5O_7$: 647.43).

1-(2-(2-Aminophenyl)-2-oxoethyl)-1,4,7,10-tetraaza cyclododecane-1,4,7-triacetic acid (DO3A-*o*AnAP). DO3A(tBu)$_3$-*o*-NH_2AP (151 mg, 0.23 mmol) was dissolved in DCM : TFA (1 : 1/v : v) and the mixture was stirred at rt overnight. After evaporation *in vacuo*, the residue was dissolved in HCl 1 M (1 ml) and evaporated *in vacuo*. The last operation was repeated twice and finally the aqueous solution was freeze dried to obtain the ligand (DO3A-AnAP) as the HCl salt in quantitative yield, without further purification (173 mg, 0.23 mmol). ^{1}H NMR (D_2O, 500 MHz): δ (ppm) = 7.85 (d, J = 6.7 Hz, –*m*-Ph–, 1H), 7.65 (t, J = 7.5 Hz, –*p*-Ph–, 1H), 7.10–7.04 (m, –*o*-Ph–, –*m*′-Ph–, 2H), 4.42–3.19 (m, macrocycle, (–NC$\underline{H}_2$COOH, –N$\underline{CH}_2$COPh, 24H). ^{13}C NMR (D_2O, 125 MHz): δ (ppm) = 203.8 (NCH$_2$$\underline{CO}$Ph), 174.3 (–NCH$_2$$\underline{CO}$OH), 160.2 (–$C_2$-Ph), 129.8 (–$C_4$-Ph–), 120.3 (–$C_6$-Ph–), 118.3 (–$C_1$-Ph), 117.9 (–$C_3$-Ph– and –$C_5$-Ph–), 59.3 (–N$\underline{C}H_2$COPh), 54.9 (–N$\underline{C}H_2$COOH), 53.5–48.32 (macrocycle). HPLC analysis (Method 1): t_r = 11.2 min. ESI-MS (m/z): found 480.41 [M + H]$^+$ (calc for $C_{22}H_{34}N_5O_7$: 480.24).

1-(2-(2-Methoxyphenyl)-2-oxoethyl)-1,4,7,10-tetraaza cyclododecane-1,4,7-triacetic acid (DO3A-*o*MeOAP). The HCl salt of DO3A-*o*-MeOAP (77 mg) was prepared following the same procedure as for the synthesis of DO3A-*o*AnAP, starting from 90 mg (0.14 mmol) of DO3A(tBu)$_3$-*o*-MeOAP. ^{1}H NMR (D_2O, 500 MHz): δ = 7.94 (d, –C_6-Ph, J = 5.6 Hz, 1H), 7.73 (t, –C_4-Ph–, J = 7.5 Hz, 1H), 7.24 (d, C_3-Ph, J = 8.5 Hz, 1H), 7.15 (t, –C_5-Ph, J = 7.5 Hz, 1H), 3.99 (s, –OC$\underline{H}_3$, 3H), 4.19–3.12 (m, macrocycle, 16H; m, –NC$\underline{H}_2$COOH, 6H, –NC$\underline{H}_2$CO–, 2H). ^{13}C NMR (D_2O, 125 Hz): δ = 192.4 (NCH$_2$$\underline{CO}$Ph), 173.9 (–NCH$_2$$\underline{CO}$OH), 160.3 (–$C_2$-Ph), 137.1 (–$C_4$-Ph–), 130.7 (–$C_6$-Ph–), 122.7 (–$C_1$-Ph–), 121.0 (–$C_5$-Ph–), 112.8 (–$C_3$-Ph–), 63.6 (–N$\underline{C}H_2$COOH), 55.7 (–O$\underline{C}H_3$), 55.09 (–N$\underline{C}H_2$COPh), 53.4–48.2 (macrocycle). HPLC analysis (Method 1): t_r = 11.4 min. ESI-MS (m/z): found 495.37 [M + H]$^+$, 248.22 [M + 2H]$^+$/2 (calc for $C_{23}H_{35}N_4O_8$:495.55).

1-(2-(4-Methoxyphenyl)-2-oxoethyl)-1,4,7,10-tetraaza cyclododecane-1,4,7-triacetic acid (DO3A-*p*MeOAP). The HCl salt of DO3A-*p*-MeOAP (75 mg) was prepared following the same procedure as for the synthesis of DO3A-*o*AnAP, starting from 90 mg (0.14 mmol) of DO3A(tBu)$_3$-*p*-MeOAP. ^{1}H NMR (D_2O, 500 MHz): δ = 7.98 (d, –$C_{2\text{-}6}$-Ph, J = 8.5 Hz, 2H), 7.12 (d, $C_{3\text{-}5}$-Ph, J = 8.5 Hz, 2H), 3.93 (s, –OC$\underline{H}_3$, 3H), 4.14–3.24 (m, macrocycle, 16H; m, –NC$\underline{H}_2$COOH, 6H, –NC$\underline{H}_2$CO–, 2H). ^{13}C NMR (D_2O, 125 Hz): δ = 190.7 (NCH$_2$$\underline{CO}$Ph), 174.0 (–NCH$_2$$\underline{CO}$OH), 164.6 (–$C_4$-Ph), 130.8 (–$C_{2\text{-}6}$-Ph–), 126.4 (–$C_1$-Ph–), 114.4 (–$C_{3\text{-}5}$-Ph–), 59.3 (–N$\underline{C}H_2$COPh), 55.7 (–O$\underline{C}H_3$), 54.7 (–N$\underline{C}H_2$COOC(CH$_3$)$_3$), 53.4–48.2 (macrocycle). HPLC analysis (Method 1): t_r = 10.8 min. ESI-MS (m/z): found 495.45 [M + H]$^+$, 248.42 [M + 2H]$^+$/2 (calc for $C_{23}H_{35}N_4O_8$: 495.55).

1-(2-(2,4-Dihydroxyphenyl)-2-oxoethyl)-4,7,10-tris-(*t*-butoxy carbonylmethyl)-1,4,7,10-tetraazacyclododecane (DO3A(tBu)$_3$-DiHAP). A solution in CH_3CN (5 mL) of DO3A(tBu)$_3$ (200 mg, 0.39 mmol), K_2CO_3 (100 mg, 0.72 mmol) and 2-bromo-2′,4′-dihydroxyacetophenone (180 mg, 0.78 mmol) was stirred under N_2 atmosphere for 5 h at room temperature and then filtered. The reaction mixture was concentrated in vacuum and then purified by preparative HPLC-MS (Method 2) to obtain (DO3A-Di-HyAP) (120 mg, 0.18 mmol, 47%). ^{1}H NMR (CD_3CN, 500 MHz): δ (ppm) = 7.59 (d, J = 8.5 Hz, (–C_6-Ph–), 1H), 6.51 (d, J = 8.5 Hz, (–C_5-Ph–), 1H), 6.40 (s, (–C_3-Ph–), 1H), 3.71–3.11 (m, macrocycle, (–NC$\underline{H}_2$COOC(CH$_3$)$_3$, –N$\underline{CH}_2$COPh, 24H), 1.34 (s, (–NCH$_2$COOC(C$\underline{H}_3$)$_3$, 27H). ^{13}C NMR (CD_3CN, 125 MHz): δ (ppm) = 190.10 (NCH$_2$$\underline{CO}$Ph), 173.8 (–NCH$_2$$\underline{CO}$OC(CH$_3$)$_3$), 168.7 (–$C_4$-Ph–), 168.3 (–$C_2$Ph–), 131.7 (–$C_6$-Ph–), 115.00 (–$C_1$-Ph–), 108.90 (–$C_5$-Ph–), 102.70 (–$C_3$-Ph–), 82.0 (–(–NCH$_2$COOC(C$\underline{H}_3$)$_3$), 59.4 (–N$\underline{C}H_2$COPh), 54.3 (–N$\underline{C}H_2$COOC(CH$_3$)$_3$), 53.4–48.3 (macrocycle), 27.2 (–NCH$_2$COOC(C$\underline{H}_3$)$_3$). ESI-MS (m/z): found 665.7 [M + H]$^+$ (calc for $C_{34}H_{57}N_4O_9$: 665.40).

1-(2-(2,4-Dihydroxyphenyl)-2-oxoethyl)-1,4,7,10-tetraazacyclododecane-1,4,7-triacetic acid (DO3A-DiHAP). The HCl salt of DO3A-DiHAP (100 mg) was prepared following the same procedure as for the synthesis of DO3A-*o*AnAP, starting from 120 mg (0.18 mmol) of DO3A(tBu)$_3$-DiHAP. ^{1}H NMR (D_2O, 500 MHz): δ (ppm) = 7.69 (d, J = 8.5 Hz, –*o*-Ph–, 1H), 6.53 (d, J = 8.5 Hz, –*m*′-Ph–, 1H), 6.41 (s, –*m*-Ph–, 1H), 3.82–3.18 (m, macrocycle, –NCH$_2$COOH, –NCH$_2$COPh, 24H). ^{13}C NMR (D_2O, 125 MHz): δ (ppm) = 189.9 (NCH$_2$COPh), 173.8 (–NCH$_2$COOH), 166.70–166.72 ((–C_2-Ph–), and (–C_4-Ph–), 132.9 (–C_6-Ph–), 116.1 (–C_1-Ph–), 107.2 (–C_3-Ph–), 102.9 (–C_5-Ph–), 63.41 (–NCH$_2$COPh), 53.2 (–NCH$_2$COOH), 51.5–48.0 (macrocycle). HPLC analysis (Method 1): t_r = 11.6 min. ESI-MS (m/z): found 497.42 [M + H]$^+$, 249.2 [M + 2H]$^+$/2 (calc for $C_{22}H_{33}N_4O_9$: 497.22).

General procedure for the preparation of Ln(III) complexes

The ligands (50 mg) were dissolved in H_2O (1 mL) and $LnCl_3$ (1.1 eq.) was added maintaining the pH around 6.5–7 and the solution was stirred overnight at room temperature. The pH was then raised to 9.5 to allow precipitation of excess Ln(III) as Ln(OH)$_3$, which after 2h was centrifuged and then filtered through a 0.2 μm filter. Finally, the pH was brought back to 7 and the solution was lyophilized to obtain the pure complex.

Gd(DO3A-*o*AnAP). HPLC analysis (Method 1): t_r = 15.5 min. ESI-MS (*m*/*z*): found 635.3 $[M + H]^+$, 317.5 $[M + 2H]^+/2$ (calc for $C_{22}H_{31}GdN_5O_7$: 635.14).

Gd(DO3A-*o*MeOAP). HPLC analysis (Method 1): t_r = 10.95 min. ESI-MS (*m*/*z*): found 650.2 $[M + H]^+$, 325.6 $[M + 2H]^+/2$ (calc for $C_{23}H_{33}GdN_4O_8$: 650.14).

Gd(DO3A-*p*MeOAP). HPLC analysis (Method 1): t_r = 10.92 min. ESI-MS (*m*/*z*): found 650.4 $[M + H]^+$, 325.7 $[M + 2H]^+/2$ (calc for $C_{23}H_{33}GdN_4O_8$: 650.14).

Gd(DO3A-DiHAP). HPLC analysis (Method 1): t_r = 10.0 min. ESI-MS (*m*/*z*): found 652.4 $[M + H]^+$, 326.5 $[M + 2H]^+/2$ (calc for $C_{22}H_{30}GdN_4O_9$: 652.14).

Eu(DO3A-*o*AnAP). HPLC analysis (Method 1): t_r = 11.9 min. ESI-MS (*m*/*z*): found 628.4 $[M + H]^+$, 314.6 $[M + 2H]^+/2$ (calc for $C_{22}H_{31}EuN_5O_7$: 628.14).

Eu(DO3A-*o*MeOAP). HPLC analysis (Method 1): t_r = 12.7 min. ESI-MS (*m*/*z*): found 643.3 $[M + H]^+$, 322.92 $[M + 2H]^+/2$ (calc for $C_{23}H_{33}EuN_4O_8$: 643.14).

Eu(DO3A-*p*MeOAP). HPLC analysis (Method 1): t_r = 11.8 min. ESI-MS (*m*/*z*): found 643.3 $[M + H]^+$, 322.19 $[M + 2H]^+/2$ (calc for $C_{23}H_{33}EuN_4O_8$: 643.14).

Eu(DO3A-DiHAP). HPLC analysis (Method 1): t_r = 9.8 min. ESI-MS (*m*/*z*): found 645.5 $[M + H]^+$, 310.5 $[M + 2H^+]/2$ (calc for $C_{22}H_{30}EuN_4O_9$: 645.11).

UV-Vis and luminescence measurements

UV analyses were carried out on a Jasco V-550 dual-lamp (deuterium) and visible (xenon) spectrophotometer scanning from 700 nm to 200 nm. Solutions at known concentration of the complexes were prepared and the UV-vis spectra were recorded at different pHs intervals (pH 6–11 for the free ligand and 4–10 for its Gadolinium complex).

Steady-state emission spectra of the Eu(III) complexes were recorded with a Horiba FluoroMax Plus-P spectrofluorometer using an integration time of 0.1 s. The excitation source was a 150 W ozone-free xenon arc lamp. The instrument was equipped with a R928P photon counting emission detector and a photodiode reference detector for monitoring lamp output. Luminescence lifetimes were measured using the time correlated single photon counting module and a xenon flash lamp as excitation source. Emission quantum yields were determined using the $Cs_3[Eu(pic)_3]$ complex (pic = 2,6-dipicolinate) as reference (Φ = 24% in TRIS, pH 7.4, 7.5×10^{-5} M).[43] UV-vis absorption spectra for quantum yield determination were obtained with 0.1 cm quartz cells using a Jasco V-650 spectrometer.

Relaxometric measurements

The water proton longitudinal relaxation rates as a function of the magnetic field strength were measured in non-deuterated aqueous solutions on a Fast Field-Cycling Stelar SmarTracer relaxometer (Stelar s.r.l., Mede (PV), Italy) over a continuum of magnetic field strengths from 0.00024 to 0.25 T (corresponding to 0.01–10 MHz proton Larmor frequencies). The relaxometer operates under computer control with an absolute uncertainty in $1/T_1$ of ±1%. Additional longitudinal relaxation data in the range 20–120 MHz were obtained with a High Field NMR Relaxometer (Stelar) equipped with a superconducting magnet HS-110 at 3.0 T. The exact concentration of Gd(III) was determined by measurement of bulk magnetic susceptibility shifts of a *t*BuOH signal. Variable-temperature ^{17}O NMR measurements were recorded on a Bruker Avance III spectrometer (11.7 T) equipped with a 5 mm probe and standard temperature control unit. Aqueous solutions of the complexes containing 2.0% of the ^{17}O isotope (Cambridge Isotope) were used. The observed transverse relaxation rates were calculated from the signal width at half-height.

Computational details

DFT calculations were performed using both the pseudopotential approximation[44] and scalar relativistic calculations.[45] All pseudopotential calculations were carried out with the Gaussian 16 program package[46] and the wB97XD functional,[47] which includes empirical dispersion. We used the quasirelativistic large-core pseudopotential of the Stuttgart/Cologne group, which includes 46 + $4f^7$ electrons in the core for Gd, and the related [5s4p3d] valence basis set.[48] All other atoms were described with the standard 6-311G(d,p) basis set. Geometry optimizations were performed without restrains and frequency calculations were carried out to confirm the nature of the optimized geometries as local energy minima or saddle points. The output of frequency calculations also provided the zero-point energies and thermal terms required to calculate the enthalpy and entropy of the systems. Solvent effects (water) were considered with integral equation formalism of the polarized continuum model (IEFPCM), using the default parameters implemented in Gaussian 16.[49] Transition states were located using the synchronous transit-guided quasi-newton method (QST3).[50] An ultrafine grid was used throughout using the integral = ultrafine keyword.

Scalar relativistic calculations were performed using the second-order Douglas–Kroll–Hess method,[51] as implemented ORCA program package.[52] These calculations used the wB97X functional,[53] in combination with the SARC2-DKH-QZVP[54] basis set for Gd and the DKH-def2-TZVPP[55] basis set for all other atoms. The resolution of identity and chain of spheres RIJCOSX approximation[56] was used to accelerate the calculations using the SARC2-DKH-QZVP/JK auxiliary basis set for Gd and the Autoaux[57] procedure to generate auxiliary basis sets for all other atoms. The grid settings were increased from the default values using the GridX8 keyword. Solvent effects (water) were included with the SMD solvation model[58] implemented in ORCA. Views of the structures were generated using the OLEX2 program.[59]

Conflicts of interest

There are no conflicts to declare.

Acknowledgements

The authors thank Centro de Computación de Galicia (CESGA) for providing the computer facilities. C. P.-I. and D. E.-G.

thank Xunta de Galicia (ED431B 2020/52) for generous financial support. D. E.-G. thanks Xunta de Galicia (ED431E 2018/03, IMMOCEL) for financial support. L. T. acknowledges Università del Piemonte Orientale (Ricerca locale 2019).

Notes and references

1 A. E. Merbach, L. Helm and E. Toth, *The Chemistry of Contrast Agents in Medical Magnetic Resonance Imaging*, John Wiley & Sons Ltd, 2nd edn, 2013.
2 L. Helm, J. R. Morrow, C. J. Bond, F. Carniato, M. Botta, M. Braun, Z. Baranyai, R. Pujales-Paradela, M. Regueiro-Figueroa, D. Esteban-Gómez, C. Platas-Iglesias and T. J. Scholl, in *Contrast Agents for MRI: Experimental Methods*, ed. V. C. Pierre and M. J. Allen, The Royal Society of Chemistry, 2017, ch. 2, pp. 121–242.
3 J. Wahsner, E. M. Gale, A. Rodríguez-Rodríguez and P. Caravan, *Chem. Rev.*, 2019, **119**, 957–1057.
4 P. Caravan, D. Esteban-Gómez, A. Rodríguez-Rodríguez and C. Platas-Iglesias, *Dalton Trans.*, 2019, **48**, 11161.
5 E. Boros, R. Srinivas, H. K. Kim, A. M. Raitsimring, A. V. Astashkin, O. G. Poluektov, J. Niklas, S. D. Horning, B. Tidor and P. Caravan, *Angew. Chem., Int. Ed.*, 2017, **56**, 5603–5606.
6 (*a*) L. Leone, M. Boccalon, G. Ferrauto, I. Fabian, Z. Baranyai and L. Tei, *Chem. Sci.*, 2020, **11**, 7829–7835; (*b*) I. M. Carnovale, M. L. Lolli, S. C. Serra, A. F. Mingo, R. Napolitano, V. Boi, N. Guidolin, L. Lattuada, F. Tedoldi, Z. Baranyai and S. Aime, *Chem. Commun.*, 2018, **54**, 10056–10059.
7 L. Leone, D. Esteban-Gomez, C. Platas-Iglesias, M. Milanesio and L. Tei, *Chem. Commun.*, 2019, **55**, 513–516.
8 S. Aime, M. Botta, M. Fasano, M. P. M. Marques, C. F. G. C. Geraldes, D. Pubanz and A. E. Merbach, *Inorg. Chem.*, 1997, **36**, 2059–2068.
9 C. Kumas, W. S. Fernando, P. Y. Zhao, M. Regueiro-Figueroa, G. E. Kiefer, A. F. Martins, C. Platas-Iglesias and A. D. Sherry, *Inorg. Chem.*, 2016, **55**, 9297–9305.
10 K. Binnemans, *Coord. Chem. Rev.*, 2015, **295**, 1–45.
11 A. Beeby, L. M. Bushby, D. Maffeo and J. A. G. Williams, *J. Chem. Soc., Dalton Trans.*, 2002, 48–54.
12 M. Regueiro-Figueroa, A. Nonat, G. A. Rolla, D. Esteban-Gómez, A. de Blas, T. Rodríguez-Blas, L. J. Charbonnière, M. Botta and C. Platas-Iglesias, *Chem. – Eur. J.*, 2013, **19**, 11696–11706.
13 S. Gündüz, S. Vibhute, R. Botár, F. K. Kálmán, I. Tóth, G. Tircsó, M. Regueiro-Figueroa, D. Esteban-Gómez, C. Platas-Iglesias and G. Angelovski, *Inorg. Chem.*, 2018, **57**, 5973–5986.
14 Z. Liang, C.-F. Chan, Y. Liu, W.-T. Wong, C.-S. Lee, G.-L. Law and K.-L. Wong, *RSC Adv.*, 2015, **5**, 13347–13356.
15 R. M. Supkowski and W. D. Horrocks Jr., *Inorg. Chim. Acta*, 2002, **340**, 44–48.
16 A. Beeby, I. M. Clarkson, R. S. Dickins, S. Faulkner, D. Parker, L. Royle, A. S. de Sousa, J. A. G. Williams and M. Woods, *J. Chem. Soc., Perkin Trans. 2*, 1999, 493–503.
17 M. H. V. Werts, R. T. F. Jukes and J. W. Verhoeven, *Phys. Chem. Chem. Phys.*, 2002, **4**, 1542–1548.
18 S. V. Eliseeva and J.-C. G. Bünzli, *Chem. Soc. Rev.*, 2010, **39**, 189–227.
19 R. S. Dickins, D. Parker, J. I. Bruce and D. J. Tozer, *Dalton Trans.*, 2003, 1264–1271.
20 C. H. R. Martínez and C. Dardonville, *ACS Med. Chem. Lett.*, 2013, **4**, 142–145.
21 G. Zhao, C. Lu, H. Li, Y. Xiao, W. Zhang, X. Fang, P. Wanga, X. Fang, J. Xu and W. Yang, *Inorg. Chim. Acta*, 2013, **406**, 146–152.
22 S. Quici, M. Cavazzini, M. C. Raffo, L. Armelao, G. Bottaro, G. Accorsi, C. Sabatini and F. Barigelletti, *J. Mater. Chem.*, 2006, **16**, 741–747.
23 U. Brath, S. I. Swamy, A. X. Veiga, C.-C. Tung, F. Van Petegem and M. Erdélyi, *J. Am. Chem. Soc.*, 2015, **137**, 11391–11398.
24 (*a*) M. Tropiano, A. M. Kenwright and S. Faulkner, *Chem. – Eur. J.*, 2015, **21**, 5697–5699; (*b*) Z. Liao, M. Tropiano, K. Mantulnikovs, S. Faulkner, T. Vosch and T. J. Sørensen, *Chem. Commun.*, 2015, **51**, 2372–2375.
25 K. N. Green, S. Viswanathan, F. A. Rojas-Quijano, Z. Kovacs and A. D. Sherry, *Inorg. Chem.*, 2011, **50**, 1648–1655.
26 S. Aime, M. Botta, D. Esteban-Gómez and C. Platas-Iglesias, *Mol. Phys.*, 2019, **117**, 898–909.
27 D. Delli Castelli, M. C. Caligara, M. Botta, E. Terreno and S. Aime, *Inorg. Chem.*, 2013, **52**, 7130–7138.
28 G. Ferrauto, D. Delli Castelli, L. Leone, M. Botta, S. Aime, Z. Baranyai and L. Tei, *Chem. – Eur. J.*, 2019, **25**, 4184–4193.
29 S. Zhang, Z. Kovacs, S. Burgess, S. Aime, E. Terreno and A. D. Sherry, *Chem. – Eur. J.*, 2001, **7**, 288–296.
30 R. Pujales-Paradela, T. Savic, D. Esteban-Gómez, G. Angelovski, F. Carniato, M. Botta and C. Platas-Iglesias, *Chem. – Eur. J.*, 2019, **25**, 4782–4792.
31 (*a*) T. J. Swift and R. E. Connick, *J. Chem. Phys.*, 1962, **37**, 307–320; (*b*) T. J. Swift and R. E. Connick, *J. Chem. Phys.*, 1964, **41**, 2553–2554.
32 (*a*) I. Solomon and N. Bloembergen, *J. Chem. Phys.*, 1956, **25**, 261–266; (*b*) N. Bloembergen and L. O. Morgan, *J. Chem. Phys.*, 1961, **34**, 842–850.
33 J. H. Freed, *J. Chem. Phys.*, 1978, **68**, 4034.
34 Z. Baranyai, L. Tei, G. B. Giovenzana, F. K. Kálmán and M. Botta, *Inorg. Chem.*, 2012, **51**, 2597–2607.
35 F. A. Dunand, R. S. Dickins, D. Parker and A. E. Merbach, *Chem. – Eur. J.*, 2001, **7**, 5160–5167.
36 D. Esteban-Gómez, A. de Blas, T. Rodriguez-Blas, L. Helm and C. Platas-Iglesias, *ChemPhysChem*, 2012, **13**, 3640–3650.
37 S. Karimi, G. Hunter, L. Moriggi, C. Platas-Iglesias and L. Helm, *Inorg. Chem.*, 2016, **55**, 6231–6239.
38 M. Regueiro-Figueroa and C. Platas-Iglesias, *J. Phys. Chem. A*, 2015, **119**, 6436–6445.
39 R. F. W. Bader and C. Chang, *J. Phys. Chem.*, 1989, **93**, 2946–2956; M. J. G. Moa and R. A. Mosquera, *J. Phys. Chem. A*, 2006, **110**, 5934–5941.
40 (*a*) B. C. Webber, K. M. Payne, L. N. Rust, C. Cassino, F. Carniato, T. McCormick, M. Botta and M. Woods, *Inorg.*

Chem., 2020, **59**, 9037–9046; (*b*) M. Woods, K. M. Payne, E. J. Valente, B. E. Kucera and V. G. Young Jr., *Chem. – Eur. J.*, 2019, **25**, 9997–10005.

41 (*a*) O. A. Blackburn, J. D. Routledge, L. B. Jennings, N. H. Rees, A. M. Kenwright, P. D. Beer and S. Faulkner, *Dalton Trans.*, 2016, **45**, 3070–3077; (*b*) O. A. Blackburn, A. M. Kenwright, A. R. Jupp, J. M. Goicoechea, P. D. Beer and S. Faulkner, *Chem. – Eur. J.*, 2016, **22**, 8929–8936; (*c*) A. Rodríguez-Rodríguez, Á. Arnosa-Prieto, I. Brandariz, D. Esteban-Gómez and C. Platas-Iglesias, *J. Phys. Chem. A*, 2020, **124**, 1362–1371.

42 L. Helm and A. E. Merbach, *Chem. Rev.*, 2005, **105**, 1923–1959.

43 A.-S. Chauvin, F. Gumy, D. Imbert and J.-C. G. Bünzli, *Spectrosc. Lett.*, 2004, **37**, 517–532 (erratum *Spectrosc. Lett.*, 2007, **40**, 193).

44 H. Stoll, B. Metz and M. Dolg, *J. Comput. Chem.*, 2002, **23**, 767–778.

45 C. van Wüllen, *J. Comput. Chem.*, 1999, **20**, 51–62.

46 M. J. Frisch, G. W. Trucks, H. B. Schlegel, G. E. Scuseria, M. A. Robb, J. R. Cheeseman, G. Scalmani, V. Barone, G. A. Petersson, H. Nakatsuji, X. Li, M. Caricato, A. V. Marenich, J. Bloino, B. G. Janesko, R. Gomperts, B. Mennucci, H. P. Hratchian, J. V. Ortiz, A. F. Izmaylov, J. L. Sonnenberg, D. Williams-Young, F. Ding, F. Lipparini, F. Egidi, J. Goings, B. Peng, A. Petrone, T. Henderson, D. Ranasinghe, V. G. Zakrzewski, J. Gao, N. Rega, G. Zheng, W. Liang, M. Hada, M. Ehara, K. Toyota, R. Fukuda, J. Hasegawa, M. Ishida, T. Nakajima, Y. Honda, O. Kitao, H. Nakai, T. Vreven, K. Throssell, J. A. Montgomery Jr., J. E. Peralta, F. Ogliaro, M. J. Bearpark, J. J. Heyd, E. N. Brothers, K. N. Kudin, V. N. Staroverov, T. A. Keith, R. Kobayashi, J. Normand, K. Raghavachari, A. P. Rendell, J. C. Burant, S. S. Iyengar, J. Tomasi, M. Cossi, J. M. Millam, M. Klene, C. Adamo, R. Cammi, J. W. Ochterski, R. L. Martin, K. Morokuma, O. Farkas, J. B. Foresman and D. J. Fox, *Gaussian 16, Revision B.01*, Gaussian, Inc., Wallingford CT, 2016.

47 J.-D. Chai and M. Head-Gordon, *Phys. Chem. Chem. Phys.*, 2008, **10**, 6615–6620.

48 M. Dolg, H. Stoll, A. Savin and H. Preuss, *Theor. Chim. Acta*, 1989, **75**, 173–194.

49 J. Tomasi, B. Mennucci and R. Cammi, *Chem. Rev.*, 2005, **105**, 2999–3093.

50 C. Peng and H. B. Schlegel, *Isr. J. Chem.*, 1993, **33**, 449–454; C. Peng, P. Y. Ayala, H. B. Schlegel and M. J. Frisch, *J. Comput. Chem.*, 1996, **17**, 49–46.

51 M. Reiher, *Theor. Chem. Acc.*, 2006, **116**, 241–252; M. Barysz and A. J. Sadlej, *J. Mol. Struct.: THEOCHEM*, 2001, **573**, 181–200.

52 F. Neese, The ORCA Program System, *Wiley Interdiscip. Rev.: Comput. Mol. Sci.*, 2012, **2**, 73–78; F. Neese, *Wiley Interdiscip. Rev.: Comput. Mol. Sci.*, 2018, **8**, e1327.

53 J.-D. Chai and M. Head-Gordon, *J. Chem. Phys.*, 2008, **128**, 084106.

54 D. Aravena, F. Neese and D. A. Pantazis, *J. Chem. Theory Comput.*, 2016, **12**, 1148–1156.

55 F. Weigend and R. Ahlrichs, *Phys. Chem. Chem. Phys.*, 2005, **7**, 3297–3305; D. A. Pantazis, X. Y. Chen, C. R. Landis and F. Neese, *J. Chem. Theory Comput.*, 2008, **4**, 908–919.

56 F. Neese, F. Wennmohs, A. Hansen and U. Becker, *Chem. Phys.*, 2009, **356**, 98–109; S. Kossmann and F. Neese, *Chem. Phys. Lett.*, 2009, **481**, 240–243.

57 G. L. Stoychev, A. A. Auer and F. Neese, *J. Chem. Theory Comput.*, 2017, **13**, 554–562.

58 A. V. Marenich, C. J. Cramer and D. G. Truhlar, *J. Phys. Chem. B*, 2009, **113**, 6378–6396.

59 O. V. Dolomanov, L. J. Bourhis, R. J. Gildea, J. A. K. Howard and H. Puschmann, OLEX2: A complete structure solution, refinement and analysis program, *J. Appl. Crystallogr.*, 2009, **42**, 339–341.